TITLE:

An individual interneuron participates in many kinds of inhibition and spans much of the mouse visual thalamus.

AUTHORS:

Josh L. Morgan[1,2*], Jeff W. Lichtman[2]

1. Department of Ophthalmology and Visual Science and Department of Neuroscience. Washington University School of Medicine, St. Louis MO 63108.
2. Department of Molecular and Cell Biology and Center for Brain Science, Harvard University, Cambridge MA 02138

Correspondence: jlmorgan@wustl.edu, jeff@mcb.harvard.edu

Lead author: jlmorgan@wustl.edu

KEYWORDS

local interneuron, dLGN, lateral geniculate nucleus, mouse connectome, connectomics, synapse mapping, retinal ganglion cell, thalamocortical cell, multiplex, dendritic computations

SUMMARY:

In principle, one way to define the functional role of a neuron would be to identify all the synaptic input it receives and all synaptic output it confers onto its targets. With serial electron microscopy we annotated all the input synapses (862) and output synapses (626) associated with one inhibitory interneuron in the visual thalamus of the mouse. This neuron's neurites covered a broad swath of lateral geniculate nucleus and spanned multiple functionally distinct regions. Every one of its neurites formed synapses onto hundreds of thalamocortical cells of several different types. All but one small neurite also had dendrite-like properties and received input from retinal ganglion cell axons. Pre- and postsynaptic associations with other inhibitory interneurons were also distributed throughout the interneuron's territory. We observed a diverse array of local synaptic motifs and three fundamentally different types of inhibitory neurites. Many thalamocortical cells were innervated weakly by this interneuron by single *en passant* shaft synapses. But a subset of the interneuron's thalamocortical cell targets received multiple synaptic inputs from targeted inhibitory neurites that climbed along the thalamocortical cell's dendrite with an assemblage of fasciculated retinal ganglion cell axons. Because of the diverse range of synaptic relationships exhibited by this one neuron, this cell defies a single functional label and seems rather to be using extremely local synaptic processing to participate in many different functions.

INTRODUCTION

A legacy of Ramón y Cajal's analysis of Golgi stained tissue is the Neuron Doctrine that states that the nervous system is made up discrete cells that act as the functional units of the brain. Critical to this unitary function of neurons is the law of dynamic polarization that states that information flows through neurons from dendrites to soma to axon. This framework, however, breaks down when considering neurons where inputs and outputs intermingle on the same neurites. In these cases,

individual neurites of the same cell can process and transmit different signals by virtue of their distinct input and output connectivities. Neurons with intermingled inputs and outputs include amacrine cells of the vertebrate retina (Grimes, Zhang, Graydon, Kachar, & Diamond, 2010), thalamic interneurons (Carden & Bickford, 2002; Famiglietti, 1970; Morest, 1975), granule cells of the olfactory bulb (Rall, Shepherd, Reese, & Brightman, 1966) and many invertebrate neurons (Christiansen et al., 2011; Graubard & Calvin, n.d.; White, Southgate, Thomson, & Brenner, 1986). In addition, many mammalian cells with clear input neurites (i.e. dendrites) and output neurites (i.e. axons) receive some degree of axo-axonic (Strettoi, Dacheux, & Raviola, 1990) or dendro-dendritic (Hattori, McGeer, & McGeer, 1979; Sloper & Powell, 1978) innervation. To get a better idea of how to describe the circuit function of a neuron with pre- and postsynaptic mixing on its neurites we sought to identify all the presynaptic input and all the postsynaptic output of one thalamic local interneuron (LIN) known to have mixing based both on anatomical (Famiglietti, 1970; Famiglietti & Peters, 1972; Guillery, 1972; Güillery, 1969; Rafols & Valverde, 1973) and physiological (Blitz & Regehr, 2005; Cox & Sherman, 2000; Crandall & Cox, 2012, 2013; Govindaiah & Cox, 2004) studies.

Here, by using serial electron microscopy to trace out all the cell's neurites and identify all its pre- and postsynaptic sites, we sought to obtain a complete picture of the input/output connections of all the neurites of a single neuron. The results of this analysis revealed that this neuron participated in many hundreds of different neuronal interactions using many kinds of synaptic motifs that spanned many functional domains in the visual thalamus.

RESULTS:

One local interneuron projects throughout the dLGN.

We previously reconstructed the excitatory feedforward connectivity (retinal ganglion cell innervation of thalamocortical neurons) in a volume of the mouse dLGN (Morgan, Berger, Wetzel, & Lichtman, 2016). For this study, we used this same "digital tissue" (Morgan & Lichtman, 2017). Because the acquired volume is in the temporal region of the dLGN, it is innervated monocularly by retinal ganglion cells (RGC) from the contralateral eye (Jaubert-Miazza et al., 2005). In this volume there are only two types of neuronal somata: the more common excitatory thalamocortical cells (TCs) and the sparser inhibitory local interneurons (LINs). The local interneurons are easily differentiable from the thalamocortical cells by their geometry (Zhu & Lo, 1999)(Figure 1A,B), connectivity and ultrastructure (Sherman, 2004)(as described below). We chose one local interneuron for detailed analysis ("LIN1") because, based on its orientation it resided largely within the volume of the 10,000 30 nm sections (400 µm x 600 µm x 300 µm). In addition, this neuron was chosen because it is connected by synapses to the previously reconstructed excitatory network of connections between retinal ganglion cell axons and thalamocortical cells (Morgan et al., 2016). LIN1 spanned the entire depth of the dLGN (500 µm of the imaged volume and nearly the entire breadth, 400 µm) and had a total neurite length of about 6.2 millimeters. Given the ~1 mm width of the dLGN in this 32 day-old mouse, this arbor expanse covers at least half the visual field (Figure 1A). The vertical extent of this arborization means that its arbor also overlaps multiple channels of retinal input. Notably, the arbor both overlaps the core and shell regions of the dLGN. These regions delineate the important functional division between the recipient zone for direction selective RGC (shell) and primarily non-direction selective RGC (core) in mouse dLGN (Reese, 1988). Therefore, if all the neurites are synaptically connected to nearby neurons (see below), LIN1 is situated so that it has the potential to influence circuits with different functions. The wide arborization of this LIN does not appear to be exceptional; the three other LINs that we reconstructed also spanned large areas of the dLGN (Figure 1A).

Morphologically, the neurites of this cell could be divided into two distinct types (Figure 1C,D). We define *shaft neurites* as the relatively thick and straight neurites that extend for hundreds of micrometers and that are responsible for traversing most of the span of LIN1's territory. The three thick neurites emerging from the LIN1 cell body were shaft neurites. In contrast, we define *targeted neurites* as the thinner more circuitous neurites with multiple irregularly shaped swellings interlinked by thinner neurites. The targeted neurites ranged from short, single bouton spine-like neurites to long (>50 um) branched structures. Targeted neurites emerged from all regions of the shaft arborization. The reverse configuration, that is, shaft neurite emerging from targeted neurites, was not observed. Analysis of LIN1's synaptic connections revealed that the morphological designation of these neurites corresponds to two modes of connecting to the dLGN network (see below).

One local interneuron forms pre- and postsynaptic connections throughout the dLGN

To determine if this expansive LIN arbor was in fact linked by synapses to multiple regions of the dLGN, we mapped all LIN1's synapses within the 100 TB volume (Supplementary Figure 2A). We identified synapses by locating all the sites where the LIN was in close apposition to another cell and where ~40 nm diameter vesicles (putative synaptic vesicles) were clustered against one of the apposed membranes (Figure 2A-L). In terms of input, we identified 745 sites where RGC axons established synapses onto LIN1, 72 synapses onto LIN1 from other LINs, 37 synapses for which the input cell type could not be definitively identified (Figure 2). Four of the LIN inputs were autaptic synapses that LIN1 formed with itself. The number of LIN synapses presynaptic to LIN1 is likely is an undercount of the actual number because of their relatively small and relatively undifferentiated morphology (Figure 2E,G). In addition to RGC and LIN inputs, LINs are known to receive input from parabranchial brainstem axons (McCormick & Pape, 1988), pretectogeniculate neurons (Wang Bickford 2002), corticothalamic inputs (Weber, Kalil, & Behan, 1989) and other cell types. Here, we group all these inputs together as 'unidentified'. However, the most common unidentified inputs were ultrastructurally consistent with cholinergic brainstem axons, possessing large oval presynaptic boutons with dark cytosol (Erişir, Van Horn, Bickford, & Sherman, 1997). In terms of output, LIN1 established 492 synapses presynaptic to thalamocortical cells, 124 synapses presynaptic to LINs (including the four onto itself), and 28 synapses presynaptic to unidentified cell types (Figure 2). There was an average of one incoming RGC synapse per 8.4 µm of the LIN neurites and one outgoing TC synapse per 12.7 µm of neurite length, although these numbers belie the fact that the synapses were unevenly distributed (see below).

Although no part of LIN1 was myelinated, most of its surface was ensheathed by glia. This wrapping was continuous with the glial ensheathment that covered the synaptic glomeruli innervated by LIN1 (Supplementary Figure 2B). At sites where LIN1's shaft neurites formed and received synapses, the glial ensheathment typically extended up to the edges of the synaptic apposition leaving only a small gap in in the glial sheath (Supplementary Figure 2C).

Every major neurite of LIN1, both shaft and targeted, innervated thalamocortical cells and thus all of LIN1's neurites have axon-like properties: 94.3% of the arbor was within 20 µm of a site presynaptic to a thalamocortical dendrite. Although LIN1 provided presynaptic input to thalamocortical dendrites throughout its widely distributed arbor, it remained possible that the dendrites being innervated were derived from a small subset of thalamocortical neuron cell bodies that were more restricted in location or type. To determine the number and distribution of thalamocortical neuronal somata innervated by LIN1, we traced all the thalamocortical dendrites postsynaptic to LIN1 back to their cell bodies. We found 265 thalamocortical neurons innervated by LIN1. These neurons were distributed widely throughout the thalamus, but typically they were located near the sites of LIN1's inhibitory contact (median distance between a thalamocortical cell soma and a LIN1 synapse = 46 µm,

95% range 17-122 µm, n = 394 synapses, Supplemental Figure 2D). The resulting spatial distribution of thalamocortical cells innervated by the LIN, therefore, roughly follows the distribution of the LIN arbor itself (Figure 3A). We also found that both strong and weak connections to TCs could be found throughout LIN1's arbor. Sixty percent (160) of LIN1's thalamocortical cell targets received only one synapse from LIN1 (Figure 3B). However, a substantial number of LIN1's associations with thalamocortical cells were much stronger: 32% of the input to thalamocortical neurons were to TCs receiving 4 or more synapses from LIN1. The thalamocortical cells that received the strongest input from LIN1 were not concentrated in any region of the dLGN arbor. The 8 thalamocortical neurons that received the largest numbers of synapses (13,9,8,8,8,7,7,6) were distributed roughly evenly across the LIN1 arborization field (Figure 3E). The wide expanse of this arbor therefore allows this single neuron to establish strong connections to thalamocortical cells at nearly opposite ends of the dLGN in both the medio-lateral and dorso-ventral axis. Thus, this neuron provides inhibition to thalamocortical cells that have receptive fields dispersed throughout the visual field of the contralateral eye. Because these thalamocortical cells are also distributed across the depth of the dLGN they include thalamocortical cells responding to different channels of visual information (Piscopo, El-Danaf, Huberman, & Niell, 2013; Reese, 1988).

Nearly all neurites of LIN1 also received synaptic input and hence had dendrite-like properties: 86.1% of LIN1s arbor was within 20 µm of an RGC input. These inputs spanned the full depth and width of its arbor and thus the full depth and most of the width of the dLGN itself. This widespread input distribution is consistent with innervation from RGCs covering much of the visual field and from RGCs with different receptive field properties.

We did identify one rather small branch of LIN1 that was not innervated by retinal ganglion cell axons. This neurite did receive one proximal synapse that may be a cholinergic brainstem input (Erişir et al., 1997). Morphologically, this RGC input-free neurite resembles the small LIN axons previously reported in rat (Zhu & Lo, 1999). The lack of RGC innervation on this neurite was not because of spatial inaccessibility. RGC boutons did come into membrane contact with this axon-like neurite and many of these were near LIN1 synapses to thalamocortical cells. However, none of these membrane contacts were associated with the clustering of synaptic vesicles or membrane thickenings that would indicate RGC to LIN synaptic transmission. In terms of output, the axon-like branch constituted a small proportion of the total LIN1 arbor length (6% total length of 5999 µm) and was responsible for only 4% (20 TCs) of LIN1's identified output to thalamocortical cells, but a slightly larger proportion (17%; 21 LINs) of this neuron's output to other LINs. If LIN1 has an axon, this neurite would be the most likely candidate. The thalamocortical cells innervated by this neurite appeared to be functionally heterogeneous because some had small glomerular type RGC input and others had large perforated RGC boutons. Previous work suggests that these bouton types correspond to different classes of RGCs and TCs (Morgan et al., 2016).

Both pre- (n=124 synapses) and postsynaptic (n=72 synapses) connections to other LINs were distributed throughout LIN1's arbor (Figure 2E-H). The exception being the lack of LIN inputs to the RGC input-free neurite just described. The neurites connecting these synapses to the cell bodies of other LINs were much longer than those linking the traced LIN to thalamocortical cells. Indeed, many of these neurites of other LINs led outside of the imaged EM volume (Fig 3C,D). Of 17 synapses that could be traced to LIN cell bodies within the volume, the distances to those somata ranged evenly from 42 µm to 232 µm (Supplemental Figure 2F). The cell bodies of the linked LINs were found throughout the entire dLGN volume. The LIN to LIN network, is therefore even more expansive than the LIN-TC network, with cell body position having little influence on the probability that two LINs will form a synapse. Thus, at the level of cell positioning, mouse LINs do not appear to be constrained by the spatial/functional organization of the visual thalamus.

Despite the wide expanse of the dLGN innervated by LIN1, it was possible that its synapses participated in only specific functional subnetworks. For example, our previous reconstruction of the retinal input to thalamocortical neurons in this same tissue revealed several ultrastructurally distinct subnetworks that were spatially intermixed (Morgan et al., 2016). We therefore explored the connectivity of LIN1 to learn if it selectively associated with any of these previously defined subnetworks. The previously reconstructed region included two morphologically distinct groups of retinal axons (large and small bouton forming) that established synapses onto two morphologically distinct groups of thalamocortical cells: those that received perforated and those that received exclusively non-perforated RGC synapses. We found that LIN1 innervated all parts of the previously traced RGC to TC network (Figure 3F,G). In particular, LIN1 was synaptically associated with both the large and small bouton forming RGCs (Figure 3F) and both classes of thalamocortical cells (Figure 3G) . These results show that one inhibitory neuron can participate in processing visual information from many distant regions of the visual field and from multiple "parallel" streams of visual processing.

One neuron generates diverse synaptic motifs

The synaptic glomeruli of the dLGN provide spatially compact structures (<10 um) in which large numbers of synapses might influence each other's functioning (Famiglietti & Peters, 1972; Guillery & Colonnier, 1970) and several multi-neuronal synaptic motifs have been consistently described for LINs as a class (Cox & Beatty, 2017; Crandall & Cox, 2013; Hámori, Pasik, Pasik, & Szentágothai, 1974; Hirsch, Wang, Sommer, & Martinez, 2015; McCormick & Pape, 1988; Pasik, Pasik, & Hámori, 1976; Sherman, 2004; Weber et al., 1989). Because we had access to all the synapses to and from this one cell, we could see the degree to which this one neuron participated in one or more kinds of inhibitory synaptic relationships. We found a diverse array of anatomical synaptic relationships associated with LIN1 including autaptic synapses, synapses with TCs with no other input nearby, RGC-TC-LIN triadic synapses, LIN-LIN-TC triadic synapses, BS (brainstem)-LIN-TC triad synapses, one-way LIN to LIN synapses and reciprocal LIN to LIN synapses (Figure 4).

The most prevalent kind of inhibitory motif associated with LIN1 was the RGC-LIN-TC triad in which a synaptically connected LIN1 neurite and TC dendrite are both innervated by the same RGC axon, often via the same presynaptic RGC bouton (Figure 5A). This motif has the effect of shortening the duration of the excitation of a thalamocortical cell by a retinal axon by following the retinal e.p.s.p. with a LIN-based i.p.s.p. (i.e. temporal sharpening, (Blitz & Regehr, 2005)). To determine the proportion of RGC inputs onto LIN1 that were associated with synaptic triads, we randomly selected 79 of the RGC inputs to LIN1 for additional local circuit analysis. For each of these boutons, we searched the bouton and nearby RGC axon for synapses onto thalamocortical cells. We found that nearly all (94%) of the RGC boutons innervating LIN1 served a dual purpose in that they also formed synapses with thalamocortical cell dendrites. Of these dual-purpose boutons, nearly all (96%) formed a synapse onto the TC that was also innervated by LIN1 (hence a triadic motif). In almost all these triadic relationships (94%), the distance between the RGC input synapse to LIN1 and the TC output synapses from LIN1 was less than 5 µm (Figure 5B). Therefore, most (84%) of retinal input to LIN1 was associated with a compact triadic subcellular pathway of less than 5 µm. These synaptic triads, in turn, could be isolated from other synaptic motifs or clustered together with other synaptic triads (Figure 4D), often as part of synaptic glomeruli. Most of the RGC inputs that were not associated with nearby TC synapses occurred on the LIN1 neurite that projects to the dorsal shell of the dLGN (Figure 4C) suggesting that a LIN might interact differently with different parts of the dLGN.

In cases where the retinal input to LIN1 was not associated with a nearby postsynaptic thalamocortical neurite (6% of 74 sampled RGC inputs), the RGC bouton presynaptic to LIN1 was

smaller in volume and lacked the high vesicle and mitochondrial densities typical of RGC boutons associated with triads.

LIN 1 also formed a simpler motif; synapses with thalamocortical neurons in the absence of nearby RGC innervation. Many of these TC inputs were formed by the one small axon-like LIN1 neurite (mentioned earlier, Figure 4F). On the rest of the LIN1 neurites, we found that about a third (34%, 16/48 sites analyzed) of the LIN1 synapses onto TCs were formed at sites where there were no nearby RGC input synapses. These LIN1 to thalamocortical neuron synapses lacking an associated RGC input were most often found on the shaft neurites of LIN1.

The lack of RGC input on the axon-like neurite necessarily means that its profile of synaptic motifs will be distinct from those of the other neurites. Interestingly, in the absence of RGC input, the LIN1 neurite often played an RGC-like role in LIN-LIN-TC synaptic motifs (Figure 4H). LIN1 boutons of the axon-like neurite formed nearby synapses onto both a thalamocortical neuron and a presynaptic dendrite of another LIN. These neurites then also innervated the same thalamocortical dendrite. The function of such a disinhibitory triad is unclear to us, but it is possible that such a motif could play an analogous role to RGC triads, temporally refining the LIN1s inhibition to a subset of its target cells.

We observed a few instances in LIN1 of vesicle clustering at contact sites with RGC boutons that innervated LIN1. While such feedback would be consistent with some previous reports (Chen & Regehr, 2003), the frequency and level of ultrastructural differentiation of these sites is insufficient for us to claim that LIN1 provided substantial reciprocal inhibition to RGCs.

Between LINs, we observed every possible combination of local synaptic motifs. These motifs included simple one-way inhibition, reciprocal synapses, and synaptic triads (the latter described above). Twenty of the 124 LIN1 inputs to other LINs were associated with reciprocal synapses form the postsynaptic LIN. At the reciprocal sites small active zones of the two cells were immediately adjacent (< 1 µm between them) (Figure 2E,G). At four of these sites LIN1 synapsed with itself (i.e., autapses). The pre- and postsynaptic sites of these autaptic synapses were separated by less than 10 µm of arbor length and so are unlikely to constitute contacts between different domains (in a functional sense) of the same cell. We also checked whether the two sides of reciprocal and autaptic synapses were consistently innervated by either the same RGC bouton or innervated the same thalamocortical dendrite (reciprocal triads). While we observed both motifs associated with LIN1, we also observed reciprocal synapses with no nearby common partner.

Five percent of the presynaptic inputs to LIN1 were neither from RGCs nor other LINs. Most of these inputs arose from large boutons consistent with brain stem inputs described previously (Erişir et al., 1997). Many of these large boutons also innervated a TC dendrite that was innervated by LIN1, thereby forming a brainstem-LIN-TC triadic motif (Figure 4B, also described previously in cat (Sherman, 2004)). The one brainstem synapse that innervated the axon-like neurite of LIN1 was notable because that synaptic bouton innervated a neurite of another LIN that was also innervated by the LIN1 axon. Such a synaptic relationship had been suggested by physiological evidence from cat dLGN (Cox & Sherman, 2000).

LIN1 therefore, engaged in many different synaptic relationships with many kinds partners. LIN1 formed triadic synaptic motifs with each type of input that formed synapses on its arbor. Variation in LIN-LIN connections seemed to cover every possible permutation of local connectivity patterns. While RGC inputs were more consistent in forming triad synapses, there was considerable variation in whether these triads were simple isolated motifs or part of much larger, more complicated arrangements of multiple RGCs, TCs and LINs (described below).

One local interneuron exhibits three distinct output modes

The range of synaptic motifs associated with this one interneuron was related to connectivity differences between the shaft and targeted neurites (anatomy described above). The thick, shaft neurites did both form and receive synapses. However, the connections occurred without any change in the path of the pre or postsynaptic neurite and often without any morphological differentiation such as bouton or spine (Figure 6). Where these shaft neurites passed through RGC synaptic glomeruli, they participated in synaptic triads, (as described above). However, most shaft synapses were not triads, but occurred at sites where LIN1 happened to be adjacent to a thalamocortical cell dendrite in the absence of an RGC input (Figure 6A). These non-triadic synapses often occurred when the LIN shaft dendrite contacted a distal dendrite of a TC, regions where RGC synapses are typically rare (Morgan et al., 2016). This lack of morphological differentiation suggests that the formation of the synapses associated with shaft neurites is incidental, occurring when LINs happen to be adjacent to thalamocortical dendrites or RGC axons rather than by directed growth of the pre- or postsynaptic partners to a common site. In terms of circuit connectivity, these shaft synapses therefore provide weak (single synapses per neurite) and diffuse (untargeted) input to the thalamocortical cells of whichever region of the dLGN they happen to pass through (Figure 6B).

In contrast to the straight paths of the shaft branches, reconstruction of the synaptic partners of targeted neurites revealed that their circuitous path reflected fasciculation with RGC axons (but not brainstem axons) and thalamocortical neuron dendrites. In this way targeted neurites brought LIN1 into extended contact with specific subsets of thalamocortical neuron dendrites and bundles of RGC axons (Figure 6C). Like observations of the presynaptic boutons of cat (Hamos et al., 1985), LIN1 targeted neurites could form multiple short side branches to fill synaptic glomeruli with synaptic boutons. However, these bundles of RGC and LIN neurites also extended beyond individual synaptic glomeruli to include multiple TCs. The fasciculated bundles of the LIN neurites, retinal axons and thalamocortical dendrites were replete with synapses (Figure 6C,D) so that synaptic partners were often connected by multiple synapses and most neurites participated in multiple triadic motifs (Figure 6D).

The morphological specificity of the targeted neurites, therefore, has three important consequences for LIN connectivity. The first is that the distribution of different kinds of connections across the LIN1 arbor is not continuous. Rather, individual targeted neurites have strong, targeted connections with cohorts of synaptic partners that are distinct from the cohorts of other neurites of LIN1. This strong, neurite-specific connectivity is consistent with the idea that neurites of LINs are functionally autonomous. The second consequence is that, even when the triadic motif fails to form at the ultrastructural scale (< 2um), the motif is still likely to occur multiple times as part of the local microcircuit organization (< 10 um). Finally, the feedforward inhibition of the triad synapse onto targeted neurites is part of a larger microcircuit motif that involves the convergence of *multiple* RGC axons onto a neurite that then delivers inhibitory input onto the target dendrites of those RGCs.

DISCUSSION

Local interneurons in the dLGN have been studied for decades in a range of species including cats, primates and rodents. Our observations are broadly consistent with many of the conclusions reached in this body of work. What is new here is that by doing circuit-scale serial electron microscopy we could assess almost all the pre- and postsynaptic interactions of an individual interneuron. We found that the diverse range of functional attributes and synaptic relationships attributed to interneurons in the visual thalamus as a class, remarkably, were present among the neurites of one single neuron. At a macroscopic level, the neuron we analyzed had synaptic associations across

different functional and retinotopic domains. At the microscopic level, it utilized a diverse set of inhibitory synaptic motifs that included not only every type of inhibition previously described in the visual thalamus, but also several motifs that seemed novel. In sum, we find it difficult to assign a particular unitary role of this interneuron because it participated in almost every conceivable kind of inhibition with every cell type and throughout many parts of the dLGN.

This neuron was atypical relative to canonical mammalian neurons in that all of its neurites had extensive axon-like presynaptic functions and all of its neurites received some synaptic input and hence had postsynaptic properties. Nonetheless one small branch seemed more axon-like than the rest because it lacked presynaptic input from retinal axons. However, what seemed like an even more important subdivision among its branches was that some of this neuron's neurites were highly targeted to associate with a cohort of thalamocortical dendrites and RGC axons while other of its neurites seemed less specific, in that they provided inhibition to TC dendrites that happened to be juxtaposed.

Global promiscuity vs. local specificity

At several spatial scales, the connectivity of this local interneuron was promiscuous. This neuron sent presynaptic dendrites throughout the dLGN and seemed like it could establish synapses with any neuron it encountered. At the level of region-to-region connectivity, its neurites appeared to obey Peters Rule (Peters & Feldman, 1976); the probability of synaptic connection within a region was reliably predicted by this neuron's arbor. The broadly distributed arborizations observed here and in other studies of rodent LINs (Seabrook, Krahe, Govindaiah, & Guido, 2013; Zhu & Lo, 1999) therefore reflect inhibitory circuitry of one neuron affecting both multiple functional channels of visual information as well as multiple regions of visual space. At a finer scale however, the connectivity pattern of this LIN was more specific. This specificity was achieved by morphological targeting of some of its neurites that gave rise to neurite-specific wiring. In particular, LIN1, in addition to its straight neurites, possessed long tortuous side branches that followed the same synaptic partners over long distances to establish multiple synaptic associations with them. The small diameters of these tortuous neurites suggest that any postsynaptic potentials within these neurites would attenuate over short distances. The combination of this electrical isolation (due to small caliber) and neurite-specific wiring suggest that these neurites operate as an array of independent computational units.

Insight into what these units are trying to accomplish may be revealed by their synaptic organization. The fasciculation of each LIN1 targeted side branch with multiple RGC axons meant that feedforward triadic motifs of many RGC axons passed through the same local patch of LIN1 neurite and TC dendrite. This local convergence of multiple RGC axons raises the possibility of a more complex role for the RGC-LIN-TC triadic synapse as being a component of a larger synaptic ensemble. Individual RGC-LIN-TC triads are thought to increase the temporal precision of TC responses to RGC input by immediately following RGC excitation with LIN inhibition (Blitz & Regehr, 2005). The window in which a thalamocortical cell might spike in response to an RGC spike is therefore kept relatively narrow. On these targeted neurites however, it is possible that this temporal filtering would affect the way signals from the many RGCs that converge on the same TC dendrite are integrated. When RGCs spike at the same time, the membrane depolarizations on the TC dendrite driven by multiple RGCs will sum together followed by the inhibitory potential from the LIN. On the other hand, when the RGCs are not synchronous, their temporally offset spikes will produce overlapping excitation and inhibition. Synchronously firing convergent RGCs would, therefore, be expected to be much more effective at driving TCs than asynchronously firing RGCs. Given that one of the primary sources of synchronous spiking in RGCs are visual events (Usrey & Reid, 1999), these dLGN microcircuits might therefore be expected to selectively pass visual events over network noise. The potential for local microcircuits to selectively pass coincident spikes is made more interesting by the observation that nearby RGC boutons

tend to share similar feature selectivities even though they are not always of the same RGC subtype (L. Liang, A. Fratzl, G. Goldey, R. N. Ramesh, A. U. Sugden, J.L. Morgan, C. Chen, 2018). The convergence of RGCs with diverse but overlapping receptive field properties on the same TC side branch therefore should produce responses in TCs that are selective to the spatial and feature overlap of the converging RGCs. In this sense, the multisynaptic motif observed in our serial electron microscopy data could generate receptive field properties that are more refined that those in the RGCs themselves.

One neuron, many functions.

The most remarkable thing about LIN1 was not the specific synaptic motifs we observed, but that so many distinct synaptic relationships were observed within a single neuron. Because locally integrated signals can be transmitted on a neurite-by-neurite basis in LIN1, this diversity in connections does not necessarily mean that LIN1 has a complex ensemble function, but rather that LIN1 performs many different functions. The combination of the capacity for local transmission of signals, the multi-region arborization, and the range on microcircuit motifs found along its arbor means it is difficult to count the number of visual computations this one neuron may participate in.

The emphasis on cell-centric organization in the nervous system is one of the principle doctrinal ideas of Cajal (and interestingly strongly disputed by his co-Nobelist, Golgi). If function is divisible into local independent sites then the fact that all these sites are associated with the same cell (i.e., supported by the same nucleus and cell body synthetic machinery) may be tangential to their function. In these cases, the neuron doctrine hides the actual computation complexity of the circuit. In transitioning from the analysis of region to region computations of Golgi type 1 cells (long axon) to the local computations of Golgi type 2 cells (short or no axon), a more neuropil-centric approach is required.

ACKNOWLEDGEMENTS:

The alignment of the mouse dLGN 3D EM dataset was performed by Art Wetzel at Pittsburgh Supercomputing. We gratefully acknowledge support from the NIH/NINDS (1DP2OD006514-01, TR01 1R01NS076467-01, and 1U01NS090449-01), Conte (1P50MH094271-01), MURI Army Research Office (contract no. W911NF1210594 and IIS-1447786), NSF (OIA-1125087 and IIS-1110955), the Human Frontier Science Program (RGP0051/2014), the NIH and NIGMS via the National Center for Multiscale Modeling of Biological Systems (P41GM10371). We are grateful to James Cuff and his expert staff at Harvard Research Computing for data management, to Hanspeter Pfister and his lab members for help with image storage and alignment, and to Richard Schalek for management and troubleshooting of the electron microscopy hardware.

AUTHOR CONTRIBUTIONS

Conceptualization, J.L.M and J.W.L.; Methodology, J.L.M.; Software, J.L.M.; Formal Analysis, J.L.M, Investigation, J.L.M; Resources, J.L.M and J.W.L.; Data Curation, J.L.M.; Writing, J.L.M and J.W.L; Visualization, J.L.M.; Funding Acquisition, J.L.M and J.W.L;

DECLARATION OF INTERESTS

The authors declare no competing interests.

REFERENCES

Blitz, D. M., & Regehr, W. G. (2005). Timing and specificity of feed-forward inhibition within the LGN. *Neuron*, *45*(6), 917–928. https://doi.org/10.1016/j.neuron.2005.01.033

Carden, W. M. B., & Bickford, M. E. (2002). Synaptic inputs of class III and class V interneurons in the cat pulvinar nucleus: Differential integration of RS and RL inputs. *Visual Neuroscience*, *19*(1), 51–59. https://doi.org/10.1017/S0952523801191054

Chen, C., & Regehr, W. G. (2003). Presynaptic modulation of the retinogeniculate synapse. *The Journal of Neuroscience : The Official Journal of the Society for Neuroscience*, *23*(8), 3130–3135. https://doi.org/23/8/3130 [pii]

Christiansen, F., Zube, C., Andlauer, T. F. M., Wichmann, C., Fouquet, W., Owald, D., … Sigrist, S. J. (2011). Presynapses in Kenyon Cell Dendrites in the Mushroom Body Calyx of Drosophila. *Journal of Neuroscience*, *31*(26), 9696–9707. https://doi.org/10.1523/JNEUROSCI.6542-10.2011

Cox, C. L., & Beatty, J. A. (2017). The multifaceted role of inhibitory interneurons in the dorsal lateral geniculate nucleus. *Visual Neuroscience*, *34*(2017), E017. https://doi.org/10.1017/S0952523817000141

Cox, C. L., & Sherman, S. M. (2000). Control of dendritic outputs of inhibitory interneurons in the lateral geniculate nucleus. *Neuron*, *27*(3), 597–610. https://doi.org/10.1016/S0896-6273(00)00069-6

Crandall, S. R., & Cox, C. L. (2012). Local Dendrodendritic Inhibition Regulates Fast Synaptic Transmission in Visual Thalamus. *Journal of Neuroscience*, *32*(7), 2513–2522. https://doi.org/10.1523/JNEUROSCI.4402-11.2012

Crandall, S. R., & Cox, C. L. (2013). Thalamic microcircuits: presynaptic dendrites form two feedforward inhibitory pathways in thalamus. *Journal of Neurophysiology*, *110*(2), 470–480. https://doi.org/10.1152/jn.00559.2012

Erişir, A., Van Horn, S. C., Bickford, M. E., & Sherman, S. M. (1997). Immunocytochemistry and distribution of parabrachial terminals in the lateral geniculate nucleus of the cat: A comparison with corticogeniculate terminals. *Journal of Comparative Neurology*, *377*(4), 535–549. https://doi.org/10.1002/(SICI)1096-9861(19970127)377:4<535::AID-CNE5>3.0.CO;2-3

Famiglietti, E. V. (1970). Dendro-dendritic synapses in the lateral geniculate nucleus of the cat. *Brain Research*, *20*(2), 181–191. https://doi.org/10.1016/0006-8993(70)90287-8

Famiglietti, E. V., & Peters, A. (1972). The synaptic glomerulus and the intrinsic neuron in the dorsal lateral geniculate nucleus of the cat. *Journal of Comparative Neurology*, *144*(3), 285–333. https://doi.org/10.1002/cne.901440304

Govindaiah, & Cox, C. L. (2004). Synaptic Activation of Metabotropic Glutamate Receptors Regulates Dendritic Outputs of Thalamic Interneurons. *Neuron*, *41*(4), 611–623. https://doi.org/10.1016/S0896-6273(04)00013-3

Graubard, K., & Calvin, W. H. (n.d.). Presynaptic Dendrites: Implications of spikeless synaptic transmission and dendritic geometry.

Grimes, W. N., Zhang, J., Graydon, C. W., Kachar, B., & Diamond, J. S. (2010). Retinal Parallel Processors: More than 100 Independent Microcircuits Operate within a Single Interneuron. *Neuron*, *65*(6), 873–885. https://doi.org/10.1016/j.neuron.2010.02.028

Guillery, R. W. (1972). Experiments to determine whether retinogeniculate axons can form translaminar collateral sprouts in the dorsal lateral geniculate nucleus of the cat. *Journal of Comparative Neurology*, *146*(3), 407–419. https://doi.org/10.1002/cne.901460306

Güillery, R. W. (1969). A quantitative study of synaptic interconnections in the dorsal lateral geniculate nucleus of the cat. *Zeitschrift Fur Zellforschung Und Mikroskopische Anatomie*, *96*(1), 39–48. https://doi.org/10.1007/bf00321475

Guillery, R. W., & Colonnier, M. (1970). Synaptic patterns in the dorsal lateral geniculate nucleus of the monkey. *Zeitschrift Für Zellforschung Und Mikroskopische Anatomie*, *103*(1), 90–108. https://doi.org/10.1007/BF00335403

Hámori, J., Pasik, T., Pasik, P., & Szentágothai, J. (1974). Triadic synaptic arrangements and their possible significance in the lateral geniculate nucleus of the monkey. *Brain Research*, *80*(3), 379–393. https://doi.org/10.1016/0006-8993(74)91024-5

Hamos, J. E., Van Horn, S. C., Raczkowski, D., Uhlrich, D. J., Sherman, S. M., & James E. Hamos, Susan C. Van Horn, Denis Raczkowski, D. J. U. S. M. S. (1985). Synaptic connectivity of a local circuit neurone in lateral geniculate nucleus of the cat. *Nature*, *317*(6038), 618–621. https://doi.org/10.1038/317618a0

Hattori, T., McGeer, P. L., & McGeer, E. G. (1979). Dendro axonic neurotransmission. II. Morphological sites for the synthesis, binding and release of neurotransmitters in dopaminergic dendrites in the substantia nigra and cholinergic dendrites in the neostriatum. *Brain Research*, *170*(1), 71–83. https://doi.org/10.1016/0006-8993(79)90941-7

Hirsch, J. A., Wang, X., Sommer, F. T., & Martinez, L. M. (2015). How Inhibitory Circuits in the Thalamus Serve Vision. *Annual Review of Neuroscience*, *38*(1), 309–329. https://doi.org/10.1146/annurev-neuro-071013-014229

Jaubert-Miazza, L., Green, E., Lo, F. S., Bui, K., Mills, J., & Guido, W. (2005). Structural and functional composition of the developing retinogeniculate pathway in the mouse. *Visual Neuroscience*, *22*(5), 661–676. https://doi.org/10.1017/S0952523805225154

L. Liang, A. Fratzl, G. Goldey, R. N. Ramesh, A. U. Sugden, J.L. Morgan, C. Chen, M. L. A. (2018). A fine-scale functional logic to convergence from retina to thalamus. *Cell*, (173), 1–13.

McCormick, D. A., & Pape, H.-C. (1988). Acetylcholine inhibits identified interneurons in the cat lateral geniculate nucleus. *Nature*, *334*(6179), 246–248. https://doi.org/10.1038/334246a0

Morest, D. K. (1975). Synaptic relationships of Golgi type II cells in the medial geniculate body of the cat. *Journal of Comparative Neurology*, *162*(2), 157–193. https://doi.org/10.1002/cne.901620202

Morgan, J. L., Berger, D. R., Wetzel, A. W., & Lichtman, J. W. (2016). The Fuzzy Logic of Network Connectivity in Mouse Visual Thalamus. *Cell*, *165*(1). https://doi.org/10.1016/j.cell.2016.02.033

Morgan, J. L., & Lichtman, J. W. (2017). Digital tissue and what it may reveal about the brain. *BMC*

Biology, *15*(1). https://doi.org/10.1186/s12915-017-0436-9

Pasik, P., Pasik, T., & Hámori, J. (1976). Synapses between interneurons in the lateral geniculate nucleus of monkeys. *Experimental Brain Research*, *25*(1), 1–13. https://doi.org/10.1007/BF00237322

Peters, A., & Feldman, M. (1976). The projection of the lateral geniculate nucleus to area 17 of the rat cerebral cortex. I. General description. *Journal of Neurocytology*, *5*(1), 63–84. Retrieved from http://dx.doi.org/10.1007/BF01176183%0Apapers2://publication/doi/10.1007/BF01176183

Piscopo, D. M., El-Danaf, R. N., Huberman, A. D., & Niell, C. M. (2013). Diverse Visual Features Encoded in Mouse Lateral Geniculate Nucleus. *Journal of Neuroscience*, *33*(11), 4642–4656. https://doi.org/10.1523/JNEUROSCI.5187-12.2013

Rafols, J. A., & Valverde, F. (1973). The structure of the dorsal lateral geniculate nucleus in the mouse. A golgi and electron microscopic study. *Journal of Comparative Neurology*, *150*(3), 303–331. https://doi.org/10.1002/cne.901500305

Rall, W., Shepherd, G. M., Reese, T. S., & Brightman, M. W. (1966). Dendrodendritic synaptic pathway for inhibition in the olfactory bulb. *Experimental Neurology*, *14*(1), 44–56. https://doi.org/10.1016/0014-4886(66)90023-9

Reese, B. E. (1988). “Hidden lamination” in the dorsal lateral geniculate nucleus: the functional organization of this thalamic region in the rat. *Brain Research Reviews*. https://doi.org/10.1016/0165-0173(88)90017-3

Seabrook, T. A., Krahe, T. E., Govindaiah, G., & Guido, W. (2013). Interneurons in the mouse visual thalamus maintain a high degree of retinal convergence throughout postnatal development. *Neural Development*, *8*(1), 1–7. https://doi.org/10.1186/1749-8104-8-24

Sherman, S. M. (2004). Interneurons and triadic circuitry of the thalamus. *Trends in Neurosciences*, *27*(11), 670–675. https://doi.org/10.1016/j.tins.2004.08.003

Sloper, J. J., & Powell, T. P. (1978). Dendro-dendritic and reciprocal synapses in the primate motor cortex. *Proceedings of the Royal Society of London. Series B, Containing Papers of a Biological Character. Royal Society (Great Britain)*, *203*(1150), 23–38. https://doi.org/10.1098/rspb.1978.0088

Strettoi, E., Dacheux, R. F., & Raviola, E. L. I. (1990). Synaptic Connections of Rod Bipolar Cells i n the Inner Plexiform Layer of the Rabbit, *466*, 449–466.

Usrey, W. M., & Reid, R. C. (1999). SYNCHRONOUS ACTIVITY IN THE VISUAL SYSTEM. *Annual Review of Physiology*, *61*(1), 435–456. https://doi.org/10.1146/annurev.physiol.61.1.435

Weber, A. J., Kalil, R. E., & Behan, M. (1989). Synaptic connections between corticogeniculate axons and interneurons in the dorsal lateral geniculate nucleus of the cat. *J Comp Neurol*, *289*(1), 156–164. Retrieved from http://www.ncbi.nlm.nih.gov/htbin-post/Entrez/query?db=m&form=6&dopt=r&uid=2808759

Wetzel, A. W., Bakal, J., Dittrich, M., Hildebrand, D. G. C., Morgan, J. L., & Lichtman, J. W. (2017). Registering large volume serial-section electron microscopy image sets for neural circuit reconstruction using FFT signal whitening. In *Proceedings - Applied Imagery Pattern Recognition Workshop*. https://doi.org/10.1109/AIPR.2016.8010595

White, J. G., Southgate, E., Thomson, J. N., & Brenner, S. (1986). The Structure of the Nervous System of the Nematode Caenorhabditis elegans. *Philosophical Transactions of the Royal Society B Biological Sciences*, *314*(1165), 1–340. https://doi.org/10.1098/rstb.1986.0056

Zhu, J. J., & Lo, F. S. (1999). Three GABA receptor-mediated postsynaptic potentials in interneurons in

the rat lateral geniculate nucleus. *The Journal of Neuroscience : The Official Journal of the Society for Neuroscience*, *19*(14), 5721–5730.

FIGURE LEGENDS

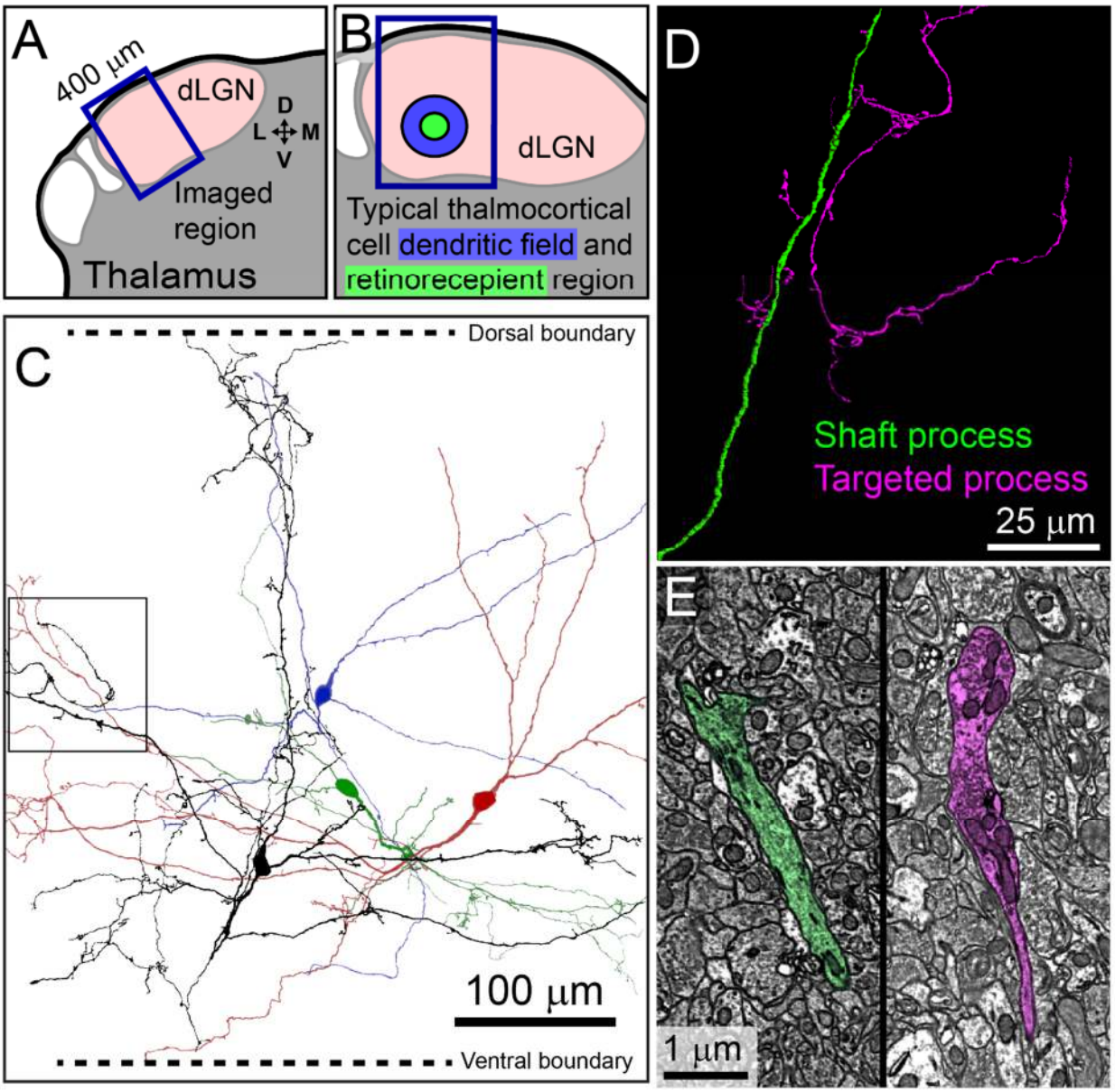

Figure 1: Morphology of dLGN LINs. A) Position of EM volume (blue box) relative to a coronal view of the dLGN (pink). B) Typical size of thalamocortical cell dendritic arbor (blue) and the proximal retinorecepient region of a thalamocortical cell (green) relative to the dLGN (pink). C) Partial tracings of four LINs showing wide dendritic arborizations. The black box is the region shown in panel D.. LIN1 is black. D) Rendering of a portion of LIN1's dendritic arbor showing the morphological differences between the shaft (green) and targeted (purple) neurites. E) Electron micrographs of shaft (green) and targeted (purple) neurites.

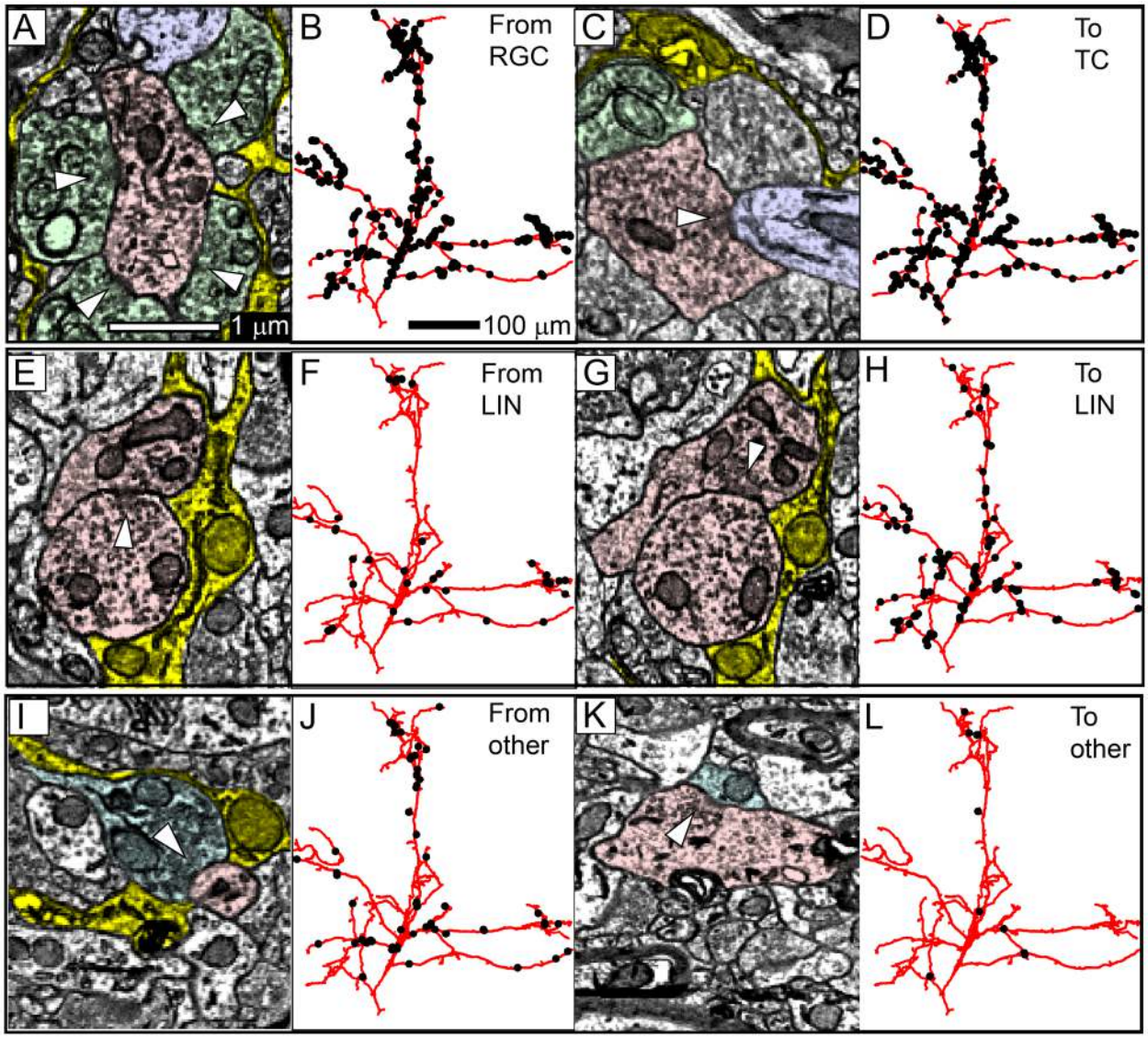

Figure 2. LIN1 forms pre and postsynaptic contacts throughout its arbor. In electron micrographs, white arrows indicate a presynaptic clustering of vesicles. Encapsulating glial sheaths are highlighted in yellow, TCs in blue, LINs in red, RGCs in green and unidentified types in cyan. A) Electron micrograph of showing RGC innervation of LIN1. B) Distribution of RGC inputs to LIN1. C) Electron micrograph showing LIN1 innervation of TC dendrite. D) Distribution of LIN1 to TC synapses. E) Electron micrograph showing LIN1 innervation of second LIN. F) Distribution of LIN1 outputs to other LINs. G) LIN input to LIN1. H) Distribution of LIN inputs to LIN1. I) Electron micrograph showing unidentified inputs onto LIN1. J) Distribution of inputs onto LIN1 from unidentified axons. K) LIN1 input onto unidentified cell type. L) Distribution of LIN1 synapses onto unidentified cell types.

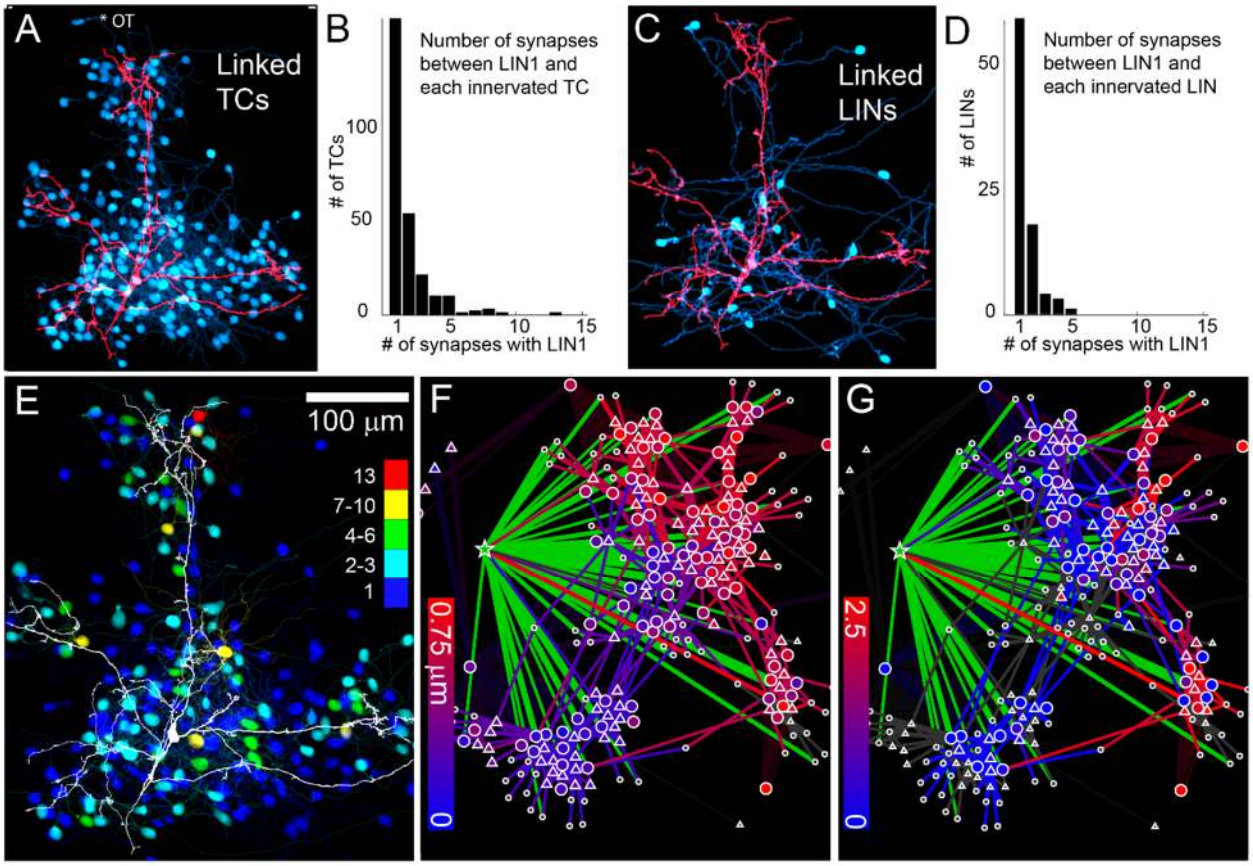

Figure 3. LIN1 connects to partners throughout the dLGN. A) Spatial distribution of cell bodies (cyan) of TCs that are innervated by LIN1 (red). B) Histogram showing that most TCs that are innervated by LIN1 receive only one or two synapses from LIN1. C) Spatial distribution of cell bodies of LINs that are synaptically connected to LIN1. Cell body positions were identified for only a small subset of LINs connected to LIN1. D) Histogram showing most LINs that are innervated by LIN1 receive only one or two synapses from LIN1. E) Spatial distribution of TCs that receive many (red, yellow) or few (blue, cyan) synapses from LIN1. F) Links of LIN1 (green star) to all clusters within a force directed sorting of a synaptically connected network of RGCs (triangles) and TCs (circles). RGC bouton diameter associated with RGCs and TCs is coded from small (blue) to large (red). G) Links of LIN1 (green star) to all clusters within a force directed network of RGCs (triangles) and TCs (circles). TC spine perforation of RGC boutons is coded from none (blue) to several (red).

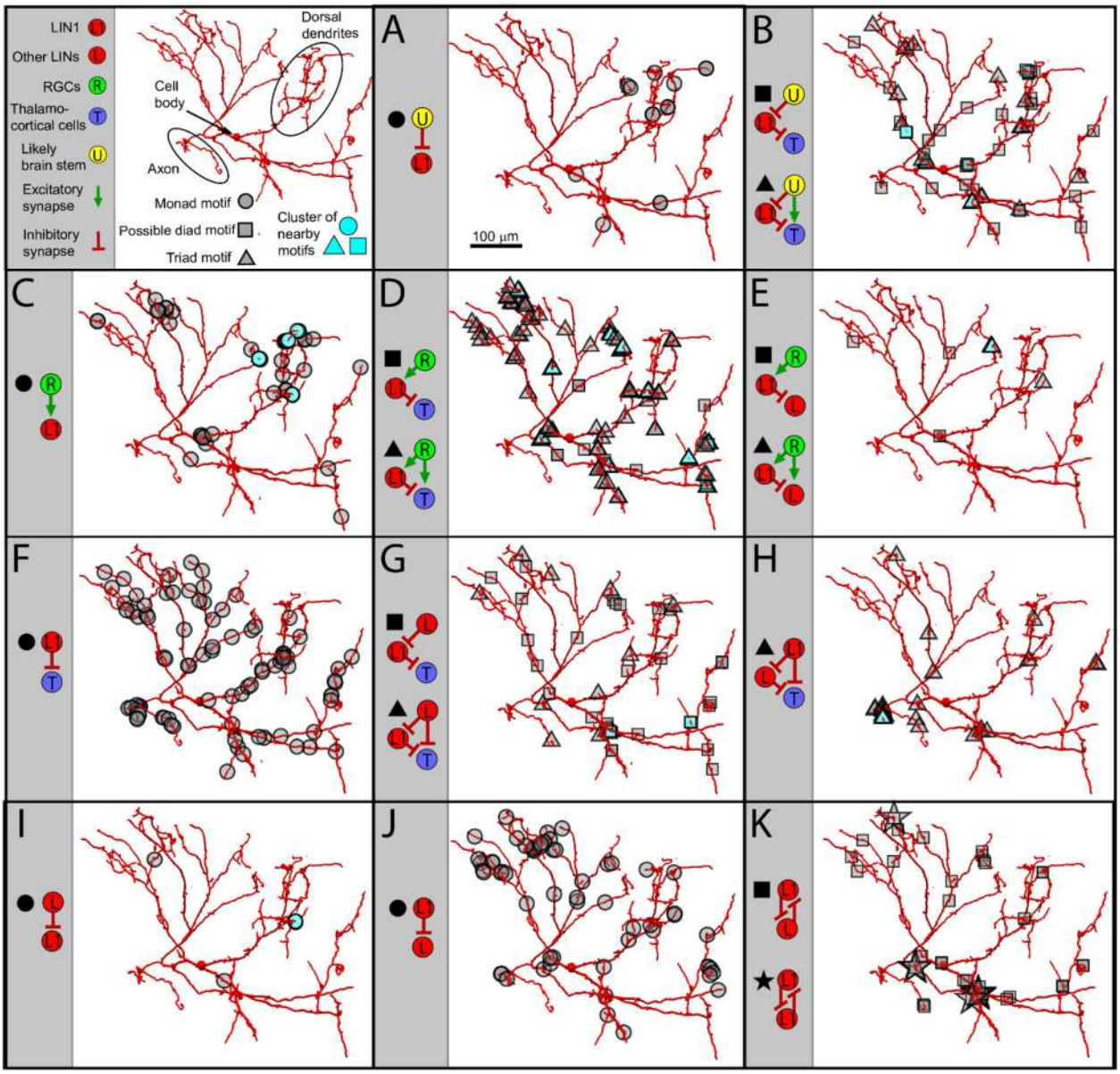

Figure 4. Synaptic motifs of LIN1. Diverse synaptic motifs were observed throughout the arbor of LIN1. LIN1 is rotated so that the axon-like neurite (see legend) is offset from the rest of the arbor. Motifs were defined as combinations of synapses found within 5 µm of one another. A clustered motif (cyan fill) is defined as a motif located less than 5 µm from at least two examples of the same motif.

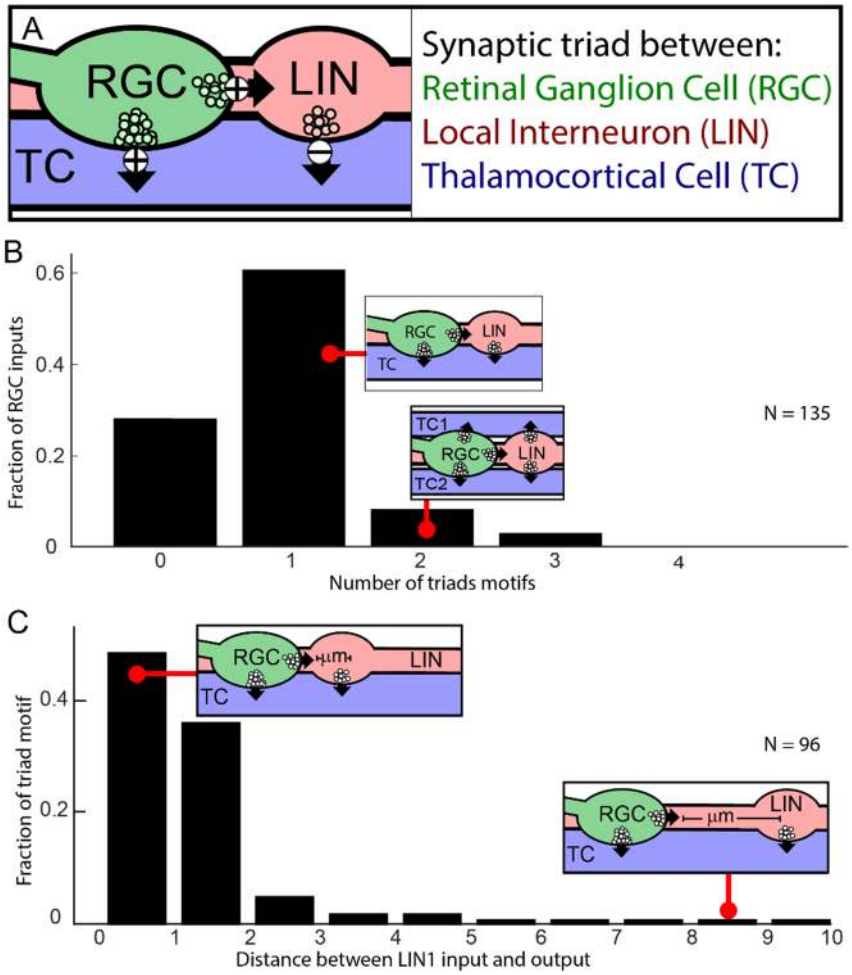

Figure 5. Structure of RGC-LIN-TC synaptic triads. A) Diagram of synaptic RGC-LIN-TC synaptic triad. Excitatory synapses = (+), Inhibitory synapses = (-)**.** B) Of 135 RGC to LIN1 synapses sampled, most are associated with a single triadic motif. To count as a triadic motif in this analysis, both the RGC-TC and LIN-TC synapse occurred within 5 µm of the RGC-TC synapse. C) In most cases where the same RGC, TC, and LIN formed synapses with each other, the synaptic input to the LIN and output from the LIN occur within a few micrometers of one another (96 triads sampled from LIN1).

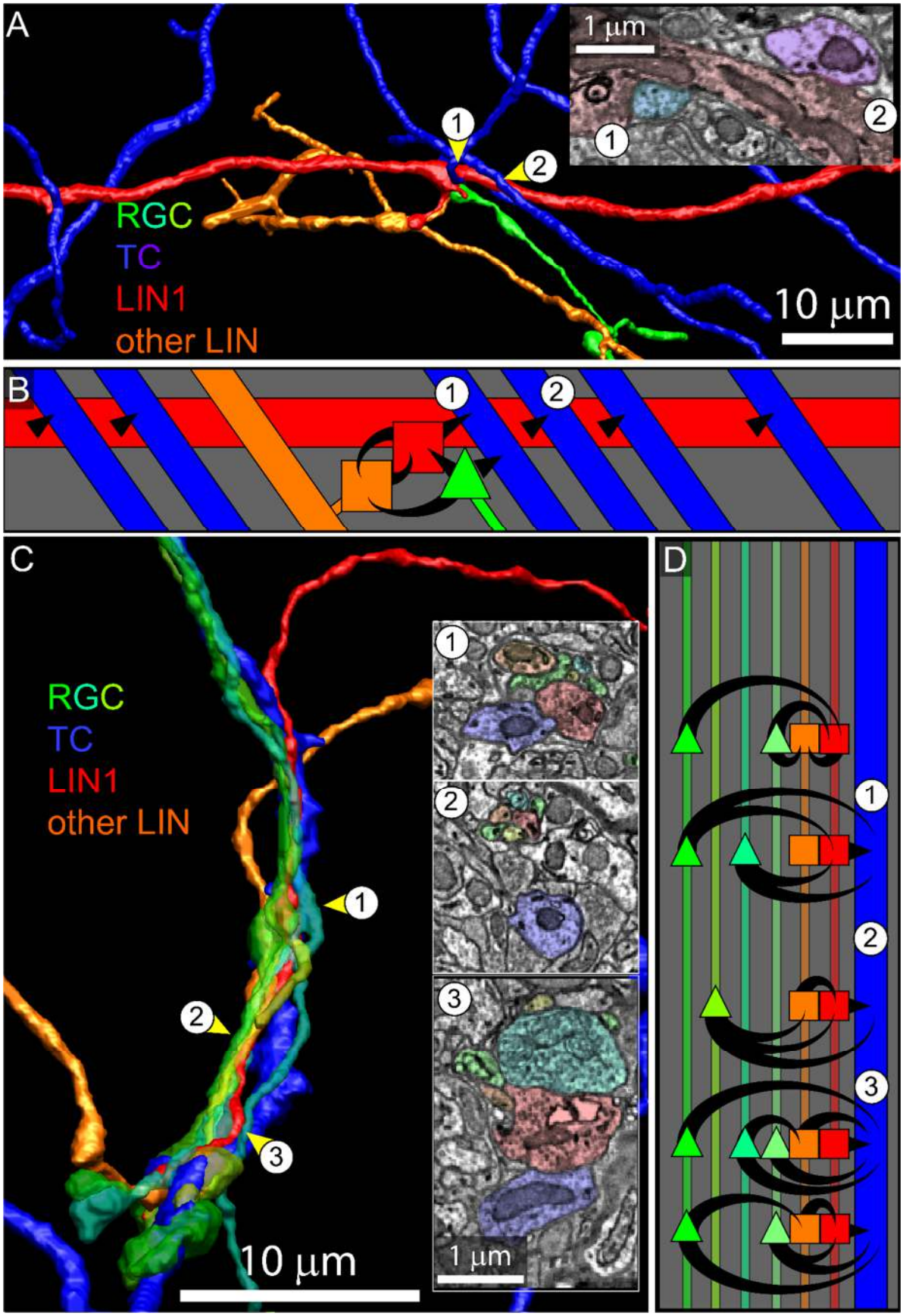
A
1 µm
1
2
RGC
TC
LIN1
other LIN
10 µm
B
C
RGC
TC
LIN1
other LIN
10 µm
1 µm
D

Figure 6. Distinct synaptic connectivities are generated by shaft and targeted neurites of LIN1. A) Rendering of a shaft presynaptic dendrite of LIN1 (red) and synaptically connected TCs (blue), LIN (orange), and RGCs (green). A short side branches of the LIN1 shaft neurite receives input from the RGC and forms reciprocal synapses with a second LIN. Circled numbers indicate the position of synapses shown in the inset electron micrograph. B) Diagram of the simple/diffuse connectivity pattern of the shaft neurite in panel A. C) Rendering of a targeted presynaptic dendrite of LIN1 (red) and synaptically connected TC (blue), LIN (orange), and four RGC axons (green, lime, cyan, yellow). All six presynaptic neurites follow the TC dendrite through the neuropil. Circled numbers indicate position of synapses shown in the inset electron micrograph. D) Diagram of the complex/strong connectivity pattern of the shaft neurite in panel A.

METHODS:

Contact for reagent and resource sharing

Further information and requests for resources and datasets should be directed to and will be fulfilled by the Lead Contact, Josh Morgan (jlmorgan@wustl.edu).

Experimental model and subject details

All animals were handled according to protocols approved by the Institutional Animal Care and Use Committee at Harvard University. Tissue from the monocular zone of the dLGN was obtained from a 32 day old C57-Blk6 mouse.

Method details

The acquisition of the dLGN EM image volume used here is described in a previous publication (Morgan et al., 2016). Briefly, a P32 C57-Blk6 mouse was anesthetized with pentobarbital and perfused with 2% paraformaldehyde plus 2% glutaraldehyde. A 300 µm vibratome slice of dLGN was stained with 2% osmium tetroxide, 0.1% thiocarbyhydrozide, 2% osmium tetroxide, and 4% uranyl acetate. The vibratome section was dehydrated with acetonitrile, embedded in Epon-Araldite and sectioned at 30 nm using ATUM. Ten thousand sections were mounted on 4 inch silicon wafers (~200 sections each) and were post-stained with 3% lead citrate. Images we acquired using the in-lens detector of a Zeiss Merlin SEM and our WaferMapper custom Matlab (Mathworks) code for automated imaging (Hayworth et al., 2014). The image stack was aligned by Art Wetzel at Pittsburgh Supercomputing (Wetzel et al., 2017). Images were acquired at 4 nm pixel size and down sampled to 16 nm pixel size for most of the image annotation. Image annotation (cell tracing, and synapse labeling) was performed manually using VAST (https://software.rc.fas.harvard.edu/lichtman/vast/).

Quantification and statistical analysis

Distances between synapses were calculated in two ways: Euclidian (3D) and topological (arbor based). Topological distances were calculated by first skeletonizing LIN1 using a shortest path algorithm described previously (Morgan et al., 2016). When searching LIN1 for synaptic motifs, we looked for groups of synapses in which the relevant LIN1 synapses were within 5 µm (topological distance) from one another. Relevant synapses not formed by LIN1 (as in the RG-TC synapse of an RGC-LIN-TC triad) were included if they occurred within 5 µm (Euclidian distance) of the relevant LIN1 synapses.

Data and software availability

All rendering and analysis was performed using custom Matlab code (Nautilus Analysis 2.3). This package of Matlab scripts imports segmentation files from VAST segmentation software and stores them as voxel lists. Cells and subcellular structures can then be retrieved individually for rendering or analysis. This code is available at https://sites.wustl.edu/morganlab/data-share/dlgn-2018/.

The dLGN dataset can be accessed at https://software.rc.fas.harvard.edu/lichtman/LGN/ and https://sites.wustl.edu/morganlab/data-share/dlgn-2018/. The segmentation files used in this publication can be accessed at https://sites.wustl.edu/morganlab/data-share/dlgn-2018/.